Choonha-Anothai *et al. Microstructures* **2025**, *5*, 2025049
DOI: 10.20517/microstructures.2024.118

Microstructures

Research Article

Open Access

Electroplating of Ni-W coating on Zn surface for durable Zn ion batteries

Khanothai Choonha-Anothai[1], Chengwu Yang[2], Meijing Wang[3], Zhiqiang Dai[3], Napat Kiatwisarnkij[1,2], Kittima Lolupiman[2,4], Xinyu Zhang[3], Panyawat Wangyao[1], Jiaqian Qin[2]

[1]Metallurgical Engineering Department, Faculty of Engineering, Chulalongkorn University, Bangkok 10330, Thailand.
[2]Center of Excellence on Advanced Materials for Energy Storage, Department of Materials Science, Faculty of Science, Chulalongkorn University, Bangkok 10330, Thailand.
[3]State Key Laboratory of Metastable Materials Science and Technology, Yanshan University, Qinhuangdao 066004, Hebei, China.
[4]Nanoscience and Technology Interdisciplinary Program, Chulalongkorn University, Bangkok 10330, Thailand.

Correspondence to: Dr. Panyawat Wangyao, Metallurgical Engineering Department, Faculty of Engineering, Chulalongkorn University, Phayathai Road, Bangkok 10330, Thailand. E-mail: panyawat.w@chula.ac.th

How to cite this article: Choonha-Anothai, K.; Yang, C.; Wang, M.; Dai, Z.; Kiatwisarnkij, N.; Lolupiman, K.; Zhang, X.; Wangyao, P.; Qin, J. Electroplating of Ni-W coating on Zn surface for durable Zn ion batteries. *Microstructures* **2025**, *5*, 2025049. https://dx.doi.org/10.20517/microstructures.2024.118

Received: 12 Nov 2024 **First Decision:** 28 Nov 2024 **Revised:** 19 Dec 2024 **Accepted:** 27 Dec 2024 **Published:** 18 Apr 2025

Academic Editors: Yuejiao Chen, Yida Deng **Copy Editor:** Fangling Lan **Production Editor:** Fangling Lan

Abstract

Aim: Aqueous zinc (Zn)-ion batteries have gained recognition as a promising energy storage solution due to their abundant zinc resources, cost-effectiveness, high energy density, and inherent safety. However, their practical application is significantly limited by issues such as dendrite formation and parasitic side reactions, which undermine the stability, efficiency, and longevity of Zn anodes. Methods: In this study, we present a novel approach by introducing a nanocrystalline nickel-tungsten (Ni-W) coating onto Zn anodes via electrodeposition. This coating acts as a functional interface, regulating Zn dissolution and deposition, suppressing dendrite growth, and minimizing side reactions. Additionally, W enhances Zn^{2+} ion adsorption, reduces nucleation energy barriers, and promotes uniform Zn growth along the Zn (002) crystallographic plane. Results: The compact morphology of the Ni-W layer further serves as a protective barrier, improving electrode stability during extended cycling. The Ni-0.1W@Zn anode demonstrates outstanding electrochemical performance, achieving over 2,000 h of stable operation at 1 mA cm^{-2} with a Coulombic efficiency of 98%. In full cell configurations paired with Ni-0.1W@Zn||V_2O_5, the system retains 81% of its capacity after 1,500 cycles at 1 A g^{-1}. Conclusion: These findings highlight the transformative potential of the Ni-W coating as a scalable and sustainable solution to address the fundamental limitations of Zn anodes, paving the way for advanced and durable energy storage technologies critical to renewable energy systems.

Keywords: Zinc-ion battery, Ni-W coating, anode, electrodeposit

INTRODUCTION

Among various metal-based secondary batteries, aqueous zinc-ion batteries (AZIBs) have emerged as a viable alternative for next-generation energy storage due to their abundance of zinc resources, cost-effectiveness, high theoretical capacity of 820 mAh g^{-1}[1-3] and inherent safety provided by aqueous electrolytes. These attributes position AZIBs as an attractive solution for large-scale renewable energy storage systems, offering environmental benefits over conventional batteries that rely on organic electrolytes. Despite their potential, AZIBs face critical challenges, particularly at the zinc anode. Dendrite formation, driven by the "tip effect" during repetitive zinc plating and stripping cycles[4-6], remains a significant issue, leading to unstable cycling behavior[7]. Furthermore, side reactions such as hydrogen evolution reactions (HER), corrosion, and passivation[8,9] reduce both efficiency and lifespan, severely limiting the commercial viability of AZIBs[10]. To mitigate these issues, several approaches have been developed[11,12], including surface modification[13-16], structural optimization[17,18], electrode engineering[19-21], and electrolyte/separator regulation[19,22], effectively reducing dendrite formation and unwanted side reactions[23-25]. These challenges necessitate the development of advanced materials and engineering strategies to stabilize the zinc anode[26,27].

Researchers have made considerable strides in improving the stability of Zn anodes through alloying and applying protective surface coatings[28]. Zinc-nickel alloys[29,30], for example, are widely recognized for their corrosion resistance and structural stability[31,32]. Their low susceptibility to hydrogen embrittlement further enhances their applicability in environments prone to degradation[33].

Among the emerging solutions, tungsten-based alloys have demonstrated remarkable potential as protective coatings in zinc-ion batteries. Tungsten offers several exceptional properties, including a high melting point (3,410 °C), low thermal expansion coefficient (4.3×10^{-6} C^{-1}), and excellent thermal conductivity (173 W/m·K), which contribute to enhanced stability and performance in demanding electrochemical environments. Its incorporation into zinc anodes provides significant benefits, such as controlling zinc deposition, suppressing dendrite growth, and improving corrosion resistance. The ability of tungsten to maintain structural integrity under repetitive plating and stripping conditions further extends the cycling life of zinc-based systems. Despite these advantages, the optimization of tungsten-to-nickel ratios and the scalable fabrication of such coatings remain underexplored[30,34-37].

In zinc-based batteries, tungsten's properties contribute significantly to improved stability and longevity. The addition of tungsten to the electrode enhances corrosion resistance, a critical factor in maintaining electrode integrity in aqueous electrolytes. Its strong bonding and high melting point help prevent structural degradation during repeated charge and discharge cycles. Furthermore, tungsten's ability to regulate zinc deposition effectively reduces dendrite formation, minimizing the risk of short circuits and extending battery lifespan[38,39].

This paper examines the effects of nickel-tungsten (Ni-W) alloy coatings on Zn foil under varying tungsten ratios while maintaining a constant nickel concentration, focusing on their impact on zinc anode stability. By promoting uniform ion transport and forming a durable alloy with zinc, Ni-W shows potential to improve both the efficiency and durability of AZIBs.

In this study, a nanocrystalline Ni-W alloy coating was developed through electrodeposition to address these challenges[40]. By forming a durable alloy with zinc, the Ni-0.1W@Zn layer enhances uniform Zn deposition and promotes controlled Zn growth along crystallographic planes. This design improves

corrosion resistance, suppresses dendrite formation, and ensures electrode stability during cycling. The Ni-0.1W@Zn anode exhibits exceptional performance, enabling symmetric cells to operate for over 2,000 h at 1 mA cm^{-2} with reduced polarization. In full-cell configurations with Zn||V_2O_5, the system achieves capacity retention exceeding 81% after 1,500 cycles at 1 A g^{-1}. The incorporation of a nanocrystalline Ni-W coating offers an innovative strategy to address the inherent challenges of Zn anodes. By enhancing Zn plating/stripping efficiency and effectively mitigating dendrite growth, this study provides a scalable and sustainable pathway for the development of high-performance Zn-ion batteries.

MATERIALS AND METHODS

Experimental details

The electrodeposition bath composition was adjusted[37-41], and deposition was conducted in galvanostatic mode using a two-electrode setup. Zinc foil, with an exposed surface area of 4 cm × 4.5 cm and a thickness of 0.1 mm, served as the cathode substrate, while a platinum electrode functioned as the anode. Ni-W coatings were plated onto the zinc foil at four concentrations (0.05, 0.1, 0.15, and 0.2 M) and for four varying durations (180, 300, 600, and 900 s). For comparison, Ni was deposited on the zinc foil at a concentration of 0.07 M. The resulting findings are summarized in Tables 1-3.

Preparation of Ni@Zn foil and Ni-W@Zn foil

Ni@Zn and Ni-W@Zn foils were prepared through constant-potential electrodeposition. Before deposition, high-purity Zn foils (99.9%) measuring 4 cm × 4.5 cm were thoroughly cleaned with acetone to remove any surface contaminants. The cleaned foil was then mounted on an acrylic plate to allow coating on one side only. Ni and Ni-W electrodeposition was performed for 180, 300, 600, and 900 s in an electrolyte solution. Deionized water was used to dilute the nickel concentration to 0.07 M, while sodium tungstate ($Na_2WO_4 \cdot 2H_2O$) was used at varying concentrations (0.05, 0.1, 0.15, and 0.2 M). Tri-Sodium Citrate Dihydrate ($Na_3C_6H_5O_7 \cdot 2H_2O$) at 0.58 M acted as a complexing agent, with Ammonium Chloride (NH_4Cl) at 0.58 M and Sodium Bromide (NaBr) at 0.2 M added to enhance conductivity. The electrodeposition setup included a Pt mesh as the counter electrode, a saturated calomel electrode (SCE) as the reference, and Zn foil as the working electrode, with a current density of 1.8 A/cm^2. After deposition, the foils were rinsed with deionized water and dried in a vacuum oven at 80 °C for 600 s to produce the Ni@Zn and Ni-W@Zn foils.

Material characterizations

The morphology of Ni@Zn foil, Ni-W@Zn foil, and bare-Zn foil was determined through scanning electron microscopy (SEM) with Energy Dispersive X-ray (EDX) mapping to determine the elemental distribution. The phase analysis of electrodes was obtained by X-ray diffraction (XRD). The optimal Ni-W@Zn samples were analyzed using X-ray Fluorescence (XRF) to determine the elemental composition of the nanoparticles. The surface roughness was identified using a confocal laser scanning microscope (CLSM).

Electrochemical measurements

The electrochemical performance tests were conducted using 2 M $ZnSO_4$ electrolyte packaged in CR2032 coin batteries. The ionic conductivity of bare-Zn, Ni@Zn, and Ni-W@Zn foils was characterized by electrochemical impedance spectroscopy (EIS) at frequencies ranging from 0.01 Hz to 100 kHz. Cyclic voltammetry (CV) tests were performed at a scan rate of 0.1 mV s^{-1} and a voltage range of 0.2-1.6 V. The Tafel curve and linear scanning voltammetry (LSV) measurements used a three-electrode system, with bare-Zn, Ni@Zn, and Ni-W@Zn as the working electrodes, platinum as the counter electrode, and Ag/AgCl as the reference electrode, respectively. The scanning rate was set to 0.1 mV s^{-1} (CHI 660e, Chenhua, China). Full cells were assembled using V_2O_5 as the cathode to evaluate the effectiveness of the Ni@Zn and Ni-W@Zn foils as anodes. The V_2O_5 cathodes were prepared by mixing the active material, conductivity agent, and PVDF binder in a weight ratio of 7:2:1, then pressed onto carbon paper using a doctor blade and dried

Table 1. Plating bath formulation and conditions for Ni-W deposition on Zinc foil

Chemicals	Bath composition [M (mol/l)]	Purpose
Nickel sulfate ($NiSO_4 \cdot 6H_2O$)	0.07	Ni source
Sodium tungstate ($Na_2WO_4 \cdot 2H_2O$)	0.05, 0.1, 0.15, 0.2	W source
Trisodium citrate dihydrate ($Na_3C_6H_5O_7 \cdot 2H_2O$)	0.58	Complexed for Ni and W
Ammonium chloride (NH_4Cl)	0.58	To increase current efficiency
Sodium bromide (NaBr)	0.2	Improve conductivity

Table 2. Plating bath formulation and conditions for Ni deposition on Zinc foil

Chemicals	Bath composition [M (mol/l)]	Purpose
Nickel sulfate ($NiSO_4 \cdot 6H_2O$)	0.07	Ni source
Sodium tungstate ($Na_2WO_4 \cdot 2H_2O$)	-	W source
Trisodium citrate dihydrate ($Na_3C_6H_5O_7 \cdot 2H_2O$)	0.58	Complexed for Ni and W
Ammonium chloride (NH_4Cl)	0.58	To increase current efficiency
Sodium bromide (NaBr)	0.2	Improve conductivity

Table 3. Electrodeposition parameters for depositing Ni and Ni-W coating on Zn foil

Parameters	Ni	Ni-W
Plating time (s)	180, 300, 600, 900	180, 300, 600, 900
Current density (A/cm^2)	1.8	1.8
Anode material	Pt mesh	Pt mesh
Temperature (°C)	25	25

under vacuum at 80 °C for 12 h. The diameter of the electrodes was 14 mm. The cell also included the integration of polypropylene microporous separators (GF/D 47 mm). Long-cycle stability during the charge-discharge process of bare-Zn, Ni@Zn, and Ni-W@Zn foil symmetrical cells was tested at 1 mA cm^{-2}. The performance of bare-Zn||Cu, Ni@Zn||Cu, and Ni-W@Zn||Cu asymmetrical cells, along with bare-Zn||V_2O_5, Ni@Zn||V_2O_5, and Ni-W@Zn||V_2O_5 full cells, was evaluated using the NEWARE system over a voltage range of 0.2-1.6 V.

RESULTS AND DISCUSSION

The electrodeposition process for a nanocrystalline Ni-W on Zn foils is outlined in Figure 1A. Ni and Ni-W electrodeposition was performed for 180, 300, 600, and 900 s in an electrolyte solution. The solutions used for Ni-W and Ni deposition, as detailed in Tables 1-3, were fully dissolved in deionized water to ensure clarity and consistency. To determine the optimal tungsten concentration and deposition time, rate performance tests were conducted to assess the electrochemical efficiency of the coatings. These tests evaluated the specific capacity across various tungsten concentrations and deposition times, providing critical insights into their correlation and performance trends. As shown in Supplementary Figure 1, the results reveal a correlation between specific capacity and both tungsten concentration and deposition time, with the combination of a 0.1 M tungsten concentration and a 300 s deposition time delivering the highest specific capacity. This outcome highlights an optimal balance between coating quality and electrochemical performance, emphasizing the importance of fine-tuning deposition parameters to achieve maximum efficiency in Zn-ion battery anodes. The optimal condition of 0.1 M tungsten concentration and 300 s deposition time provides the highest specific capacity, emphasizing the importance of deposition parameters. To evaluate the effects of tungsten concentration and deposition time, morphological analysis was conducted to examine the surface structure and coating quality of Zn electrodes. As shown in

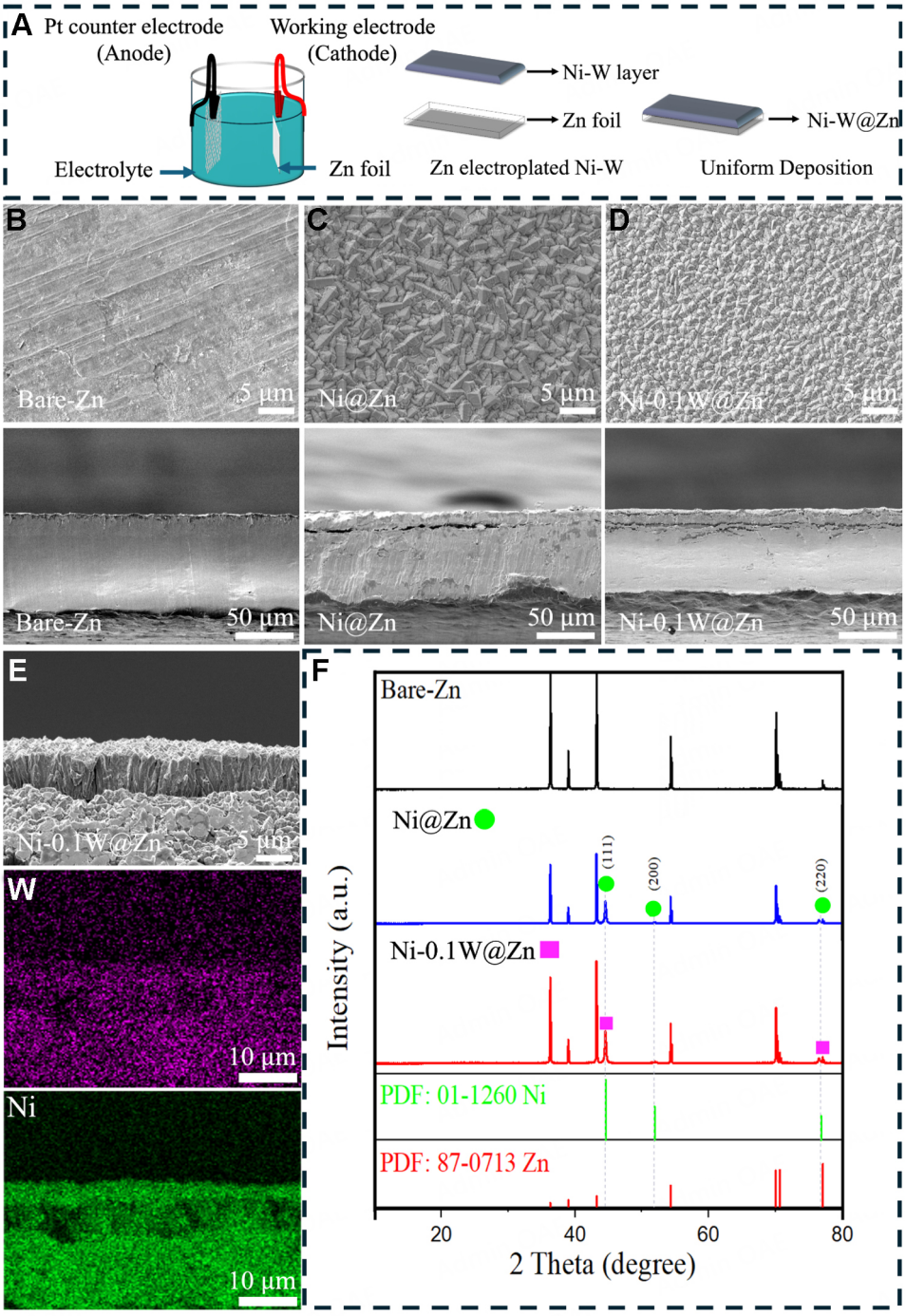

Figure 1. (A) Schematic illustration of preparation procedure and mechanism simulations of Ni-0.1W@Zn. SEM images and cross-section of (B) Bare-Zn, (C) Ni@Zn and (D) Ni-0.1W@Zn. (E) Element mapping images of Ni-0.1W@Zn. and (F) XRD patterns of Bare-Zn, Ni@Zn and Ni-0.1W@Zn.

Figure 1B, SEM images illustrate the results for deposition times of 180, 300, 600, and 900 s at a tungsten concentration of 0.1 M. At 180 s [Supplementary Figure 2], the Ni-W layer was insufficient to fully cover the Zn foil. Prolonged deposition times, such as 600 and 900 s [Supplementary Figure 3], led to the formation of tungsten oxide, resulting in non-uniform adhesion and reduced coating quality, particularly

when the tungsten concentration exceeded 0.15 M. Additionally, deposition times below 300 s were found to be suboptimal due to hydrogen gas adsorption on the Zn surface, causing surface cracks and voids [Supplementary Figure 4][42]. Optimal deposition was achieved at 180 and 300 s for both Ni and Ni-W coatings. The top-view and cross-sectional SEM images [Figure 1B-D] illustrate the structural differences among Bare-Zn, Ni@Zn (nickel concentration of 0.07 M, deposition time of 180 s), and Ni-0.1W@Zn (tungsten concentration of 0.1 M, deposition time of 300 s).

SEM characterization reveals that Ni@Zn [Figure 1C] exhibits a polygonal structure with rough facets, whereas Ni-0.1W@Zn [Figure 1D] forms a semi-spherical and more compact morphology. This distinct morphological evolution upon tungsten incorporation highlights its critical role in facilitating uniform Zn deposition and enhancing surface compactness, both of which are essential for improved cycling stability. SEM-EDX element mapping [Figure 1E and Supplementary Figure 5] confirms that Ni and W are uniformly distributed across the Ni-0.1W@Zn surface, forming a highly compact and homogeneous layer approximately 5 μm thick. XRF [Supplementary Figure 6] analysis further substantiates tungsten incorporation, revealing a tungsten content of 5.03%, indicating its successful integration within the bulk structure. Complementary energy-dispersive X-ray spectroscopy (EDS) analysis identifies a higher tungsten content of 12.51%, suggesting preferential enrichment near the coating surface. These findings not only verify the presence of tungsten but also underscore its strategic localization, which enhances Zn^{2+} ion adsorption, promotes uniform Zn deposition, and suppresses dendrite formation.

The optimized coating thickness of approximately 5 μm ensures efficient electron transport and minimizes internal resistance, critical for achieving high-performance Zn-ion batteries[43]. Tungsten incorporation significantly enhances structural stability during prolonged cycling, making Ni-0.1W@Zn highly suitable for long-term applications. In contrast, the Ni@Zn coating exhibits a considerably thicker layer (approximately 13 μm), as shown in cross-sectional SEM analysis [Supplementary Figure 7]. While providing surface coverage, this excessive thickness increases internal resistance and hinders efficient electron transport. Moreover, the absence of tungsten in Ni@Zn results in insufficient suppression of dendrite growth and limited structural stability during extended cycling. Conversely, the Ni-0.1W@Zn coating, with its optimized thickness and tungsten incorporation, delivers superior electron transport and reduced resistance, ensuring efficient Zn plating and stripping cycles[44]. These properties position Ni-0.1W@Zn as a more effective and reliable anode material for Zn-ion batteries. SEM analysis further highlights the uniform and dense morphology of the Ni-W coating, which is vital for controlling Zn deposition and mitigating dendrite growth. These structural attributes significantly enhance anode stability, addressing challenges associated with uncontrolled Zn growth during extended cycling. The optimized morphology and compositional features establish Ni-0.1W@Zn as a promising material for developing durable, high-performance energy storage systems.

Additionally, XRD analysis [Figure 1F] confirms the presence of Ni and W coatings on Zn foil. Distinct peaks are observed for the Ni (200) crystallographic plane at $2\theta = 44.52°$ in a face-centered cubic structure and for tungsten at $2\theta = 43.19°$, aligning with the Joint Committee on Powder Diffraction Standards (JCPDS). The average particle size of nickel nanoparticles, calculated from the Ni (111) peak at $2\theta = 44.54°$ using the Scherrer equation, is approximately 27 nm. The nanoscale particle size shortens diffusion paths for ions and electrons, enhancing reaction kinetics and increasing rate capability. Furthermore, the structural flexibility of nanoparticles accommodates volume changes during charge and discharge cycles, minimizing degradation and improving cycling stability. These features are particularly valuable for applications requiring high energy density and extended cycle life[45].

Figure 2A-C illustrates bare-Zn, Ni@Zn, and Ni-0.1W@Zn electrodes soaked in a 2 M $ZnSO_4$ electrolyte for 14 days to evaluate their chemical stability. The SEM images of the electrodes after soaking, as shown in Figure 2D-F, reveal a uniform surface on Ni-0.1W@Zn, whereas Zn dendrites are more pronounced on the bare-Zn and Ni@Zn surfaces. This indicates that the Ni-0.1W@Zn coating effectively minimizes Zn dendrite formation and controls crystal growth, contributing to enhanced battery longevity[46-48].

Figure 2G-I shows contact angle measurements for bare-Zn, Ni@Zn, and Ni-0.1W@Zn with 2 M $ZnSO_4$ electrolyte, measuring 110.45°, 129.63°, and 71.10°, respectively. The significantly lower contact angle of Ni-0.1W@Zn demonstrates superior wettability[49]. This increased hydrophilicity enhances electrolyte access and Zn^{2+} ion transport, which positively affects cycling performance[50]. As shown in Figure 2J, the corrosion potential of Ni-0.1W@Zn (-0.898 V) is higher than that of bare-Zn (-0.900 V) and Ni@Zn (-0.909 V), indicating improved corrosion resistance. Additionally, corrosion tests conducted in 2M $ZnSO_4$ solution demonstrate that Ni-0.1W@Zn significantly reduces corrosion current, further underscoring its durability.

To verify the positive effects of the Ni-W coating on zinc metal anodes, long-term cycling stability tests were conducted at a constant current density of 1 mA cm^{-2} and a capacity of 0.5 mAh cm^{-2}. While the initial cycles exhibited relatively high voltage polarization, the overpotential for Zn plating/stripping with Ni-0.1W@Zn||Ni-0.1W@Zn stabilized at 68.1 mV, as shown in Figure 3A and Supplementary Figure 8. Moreover, the Ni-0.1W@Zn||Ni-0.1W@Zn cell maintained stable cycling for over 2,000 h, indicating enhanced Zn^{2+} ion transport due to the Ni-W coating. In contrast, bare Zn and Ni@Zn electrodes experienced significant and irreversible voltage drops between 100 and 400 h, signaling battery failure due to short circuits caused by Zn dendrite growth. The poor electrochemical performance of Ni@Zn was further evident from the increased overpotential (114.9 mV) compared to its initial value of 96.9 mV, as shown in Figure 3B. When symmetric cells were tested at a higher current density of 2 mA cm^{-2} and a capacity of 1 mAh cm^{-2}, the Ni-0.1W@Zn||Ni-0.1W@Zn battery demonstrated stable cycling for over 1,300 h, as depicted in Figure 3C and Supplementary Figure 9. The voltage curve remained steady, with a low initial overpotential of 92.1 mV, compared to 108.2 mV for Ni@Zn. The Ni-0.1W@Zn exhibited ultralow voltage hysteresis, contrasting sharply with the poor performance of Ni@Zn, which failed within 100 h, accompanied by a sharp increase in overpotential to 146.6 mV [Figure 3D]. This was significantly higher than the 84.9 mV overpotential observed for Ni-0.1W@Zn. The low nucleation overpotential and minimal voltage hysteresis of Ni-0.1W@Zn indicate a decreased energy barrier for Zn deposition and improved Zn ion transfer kinetics[51]. The superior Coulombic efficiency (CE) and prolonged cycling lifespan of Ni-0.1W@Zn underscore its potential for advanced energy storage applications. As shown in Figure 3E, the voltage hysteresis values of bare Zn and Ni@Zn are 186 and 177 mV, respectively, indicating disordered Zn nucleation and growth. In contrast, Ni-0.1W@Zn exhibits a significantly lower overpotential of 89.5 mV, reflecting stable cycling and enhanced Zn^{2+} ion transport[52]. Additional performance tests using Cu||Zn asymmetric cells, with Cu foil as the counter electrode, were conducted at 1 mAh cm^{-2} capacity and 1 mA cm^{-2} current density. Bare Zn and Ni@Zn showed an initial CE of 98% but maintained stable cycling for only up to 150 and 400 cycles, respectively[53]. In contrast, Ni-0.1W@Zn demonstrated superior cycling reversibility, achieving a CE of 98% for up to 1,100 cycles [Figure 3F]. This performance highlights a more reversible Zn ion plating/stripping process. XRD analysis in Figure 3G reveals that Ni-0.1W@Zn retained strong diffraction peaks even after extended cycling, indicating high electrochemical stability. In comparison, bare Zn and Ni@Zn exhibited increased by-products, such as $Zn_4SO_4(OH)_6{\cdot}5H_2O$ (PDF#78-0246), a common by-product in zinc-ion batteries. This by-product formation reflects electrode surface changes due to H^+ insertion, as confirmed by a peak at 12.27° observed during discharge. Notably, Ni-0.1W@Zn generated fewer by-products even after 1,000 cycles, with prominent nickel and tungsten peaks remaining visible. Furthermore, XRD patterns indicate significant Zn crystal growth along the (100) and

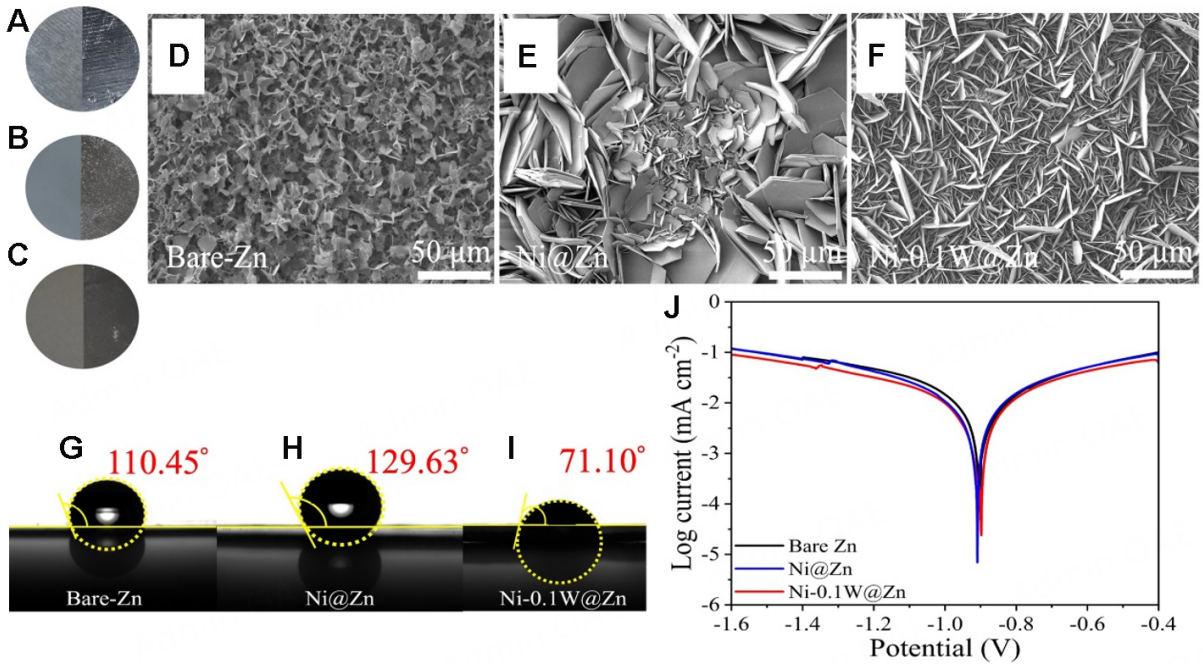

Figure 2. Optical image of initial state of (A) Bare-Zn and (B) Ni@Zn and (C) Ni-0.1W@Zn compared with after soaked and immersed in 2M $ZnSO_4$ electrolyte for 14 days. SEM images of (D) Bare-Zn, (E) Ni@Zn and (F) Ni-0.1W@Zn immersed in 2M $ZnSO_4$ electrolyte for 14 days of surface. Contact angles of (G) Bare-Zn, (H) Ni@Zn and (I) Ni-0.1W@Zn and (J) Tafel curve of Bare-Zn, Ni@Zn and Ni-0.1W@Zn.

(110) planes in bare Zn and Ni@Zn, whereas Ni-0.1W@Zn exhibited markedly reduced crystal growth in (002) planes[54], indicating enhanced structural stability[55,56]. The dissolution of Ni-0.1W@Zn and Zn deposition beneath the Ni-W layer during cycling suggests a Zn deposition mechanism involving electron transfer between $Zn(OH)_2$ and charge carriers[57]. This layer creates a potential gradient across the coating, enabling ion diffusion through the Ni-W layer [Figure 3H], and promoting uniform Zn deposition across the electrode[58]. However, uncontrolled Zn growth during extended cycling could ultimately lead to internal short circuits under the Ni layer or on bare Zn surfaces[59].

Figure 4A-C presents the morphologies of Bare-Zn, Ni@Zn, and Ni-0.1W@Zn anodes in symmetric cells at 1 mA cm^{-2}. The Bare-Zn surface exhibits an uneven texture with prominent Zn flakes and dendrites, which appear after 100 h in bare-Zn cells and after 400 h in Ni@Zn cells [Supplementary Figure 10]. These changes reflect progressive dendrite growth and surface degradation over time. In contrast, the Ni-0.1W@Zn anode retains a smooth and uniform surface even after 2,000 h, demonstrating its effectiveness in achieving consistent Zn deposition and minimizing by-product formation during plating and stripping. Further analysis, as shown in Supplementary Figure 11, examines the morphologies of Bare-Zn, Ni@Zn, and Ni-0.1W@Zn electrodes at a higher current density of 2 mA cm^{-2}. On Bare-Zn and Ni@Zn surfaces, zinc dendrites gradually grow and cluster into large protrusions due to uncontrolled Zn plating and stripping, leading to the formation of Zn flakes and unwanted side reactions. In contrast, SEM images of the Ni-0.1W@Zn anode reveal a highly uniform Zn deposition, effectively suppressing dendrite growth and reducing the occurrence of side reactions. Laser confocal microscopy in Figure 4D-F and Supplementary Figure 12 provides additional insight, revealing significant height differences on the surfaces of bare-Zn and Ni@Zn electrodes, exceeding 90 and 20 μm, respectively. By comparison, the Ni-0.1W@Zn anode exhibits much lower surface roughness (14 μm), ensuring an even distribution of Zn deposits and effectively suppressing dendrite formation.

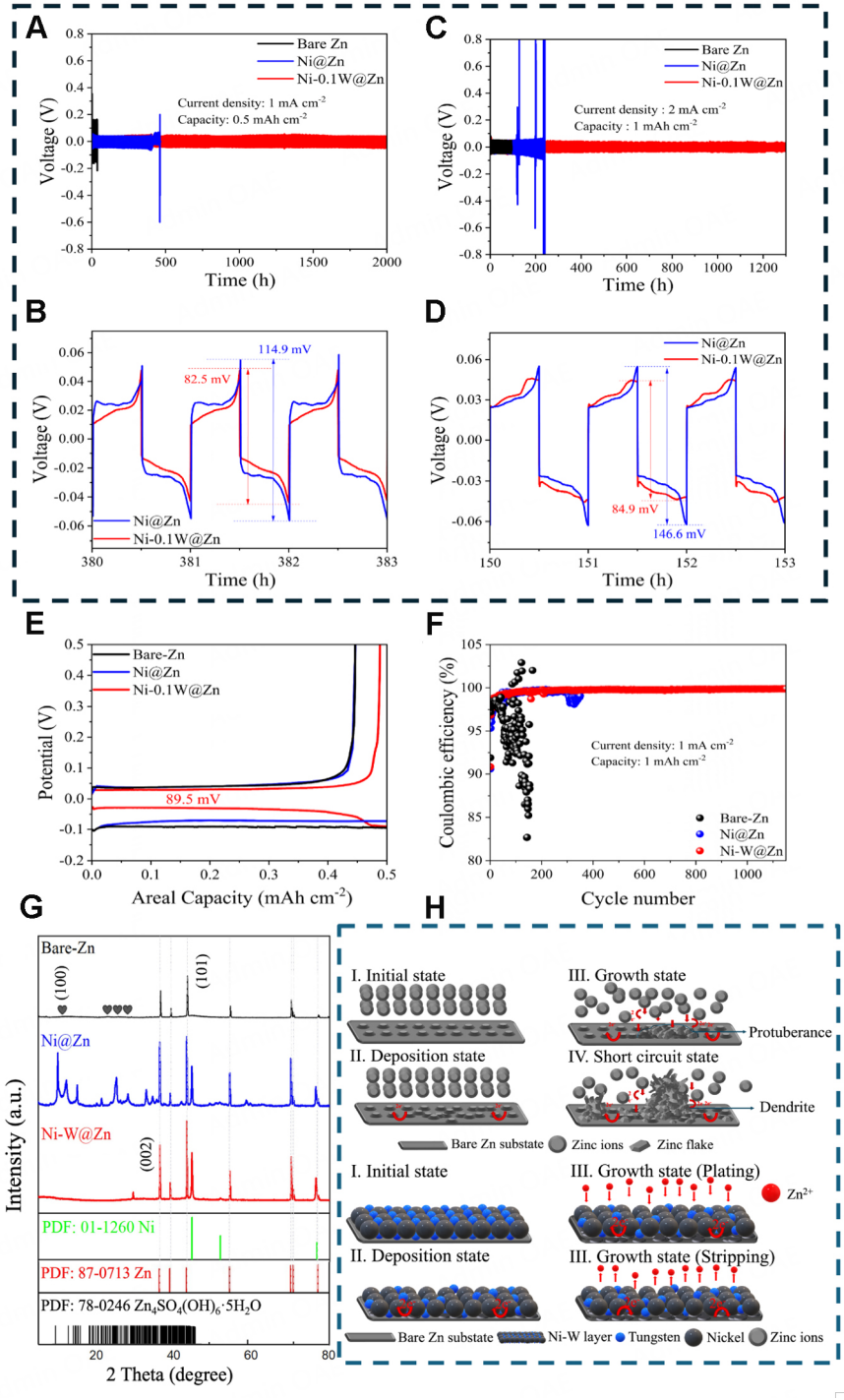

Figure 3. (A) Cycling stability of Bare-Zn, Ni@Zn and Ni-0.1W@Zn in symmetrical cells at 1 mA cm^{-2}; (B) enlarged voltage profiles of Ni@Zn and Ni-0.1W@Zn at 1 mA cm^{-2}; (C) Cycling stability of Bare-Zn, Ni@Zn and Ni-0.1W@Zn in symmetrical cells at 2 mA cm^{-2}; (D) enlarged voltage profiles of Ni@Zn and Ni-0.1W@Zn at 2 mA cm^{-2}; (E) The first curves of Cu||Zn cell, Cu||Ni@Zn and Cu||Ni-0.1W@Zn cell at 1 mA cm^{-2} for 0.5 mAh cm^{-2}; (F) Coulombic efficiency of Zn plating/stripping in Bare-Zn, Ni@Zn and Ni-0.1W@Zn cells with a current density of 1 mA cm^{-2} capacity of 1 mAh cm^{-2} (G) XRD patterns of Bare-Zn, Ni@Zn and Ni-0.1W@Zn after 200 h cycles at 1 mA cm^{-2}; Schematic illustrations of (H) Bare-Zn and (F) Ni-0.1W@Zn during plating/stripping.

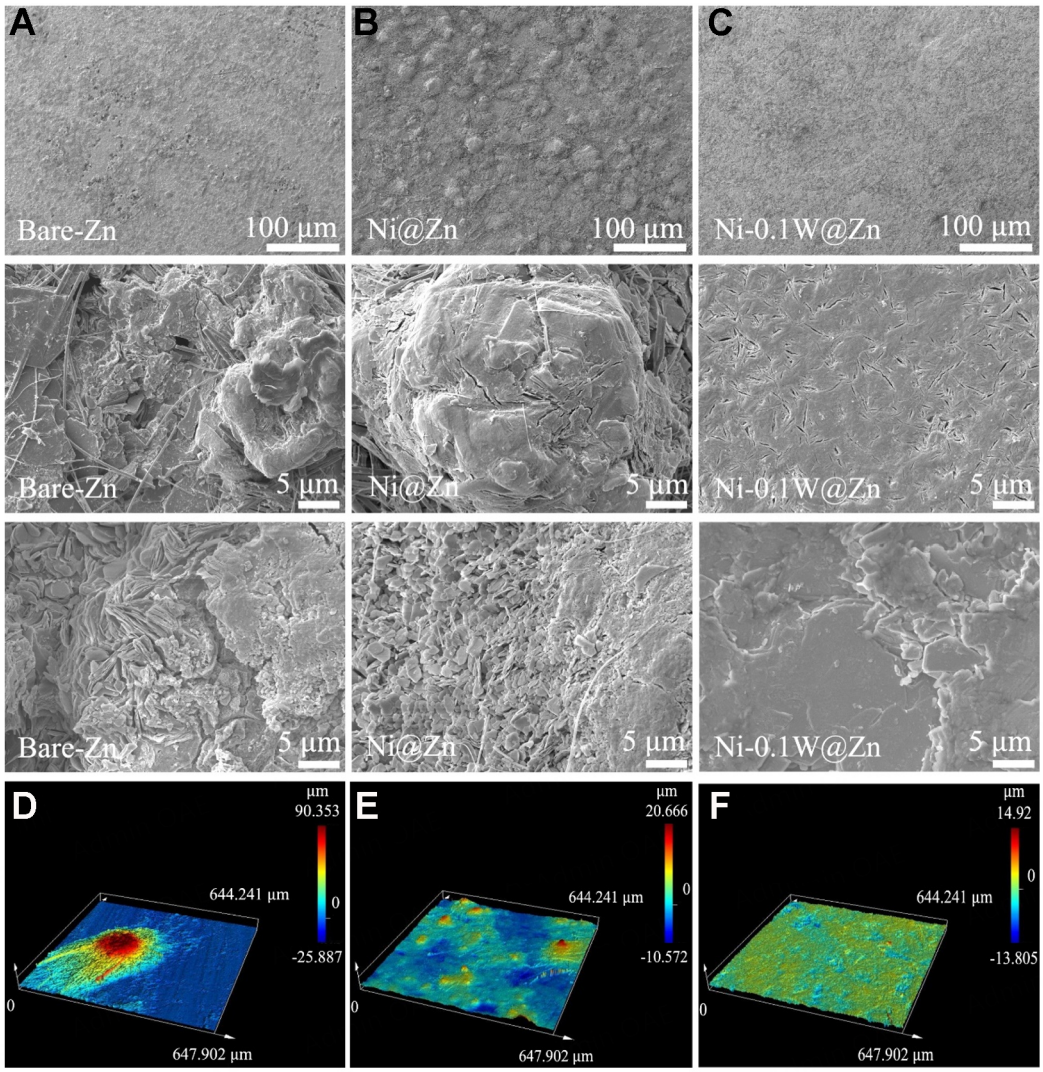

Figure 4. SEM images of (A) Bare-Zn after 100 h at 1 mA cm^{-2} and (B) Ni@Zn after 400 h at 1 mA cm^{-2} and (C) Ni-0.1W@Zn after 2,000 h at 1 mA cm^{-2}. The laser confocal microscopy images of (D) Bare-Zn (E) Ni@Zn and (F) Ni-0.1W@Zn after plating/stripping.

Further evaluation of the Ni-0.1W@Zn anode was conducted in full cells paired with V_2O_5 as the cathode, as shown in Figure 5A. CV curves at 1 mV s^{-1} demonstrate significantly enhanced electrochemical capacity in Ni-0.1W@Zn||V_2O_5 cells. The Nyquist plots for full cells using bare-Zn, Ni@Zn, and Ni-0.1W@Zn anodes, tested before and after cycling [Figure 5B], reveal that the charge transfer resistance of bare-Zn (119.0 Ω) and Ni@Zn (90.0 Ω) is markedly higher than that of Ni-0.1W@Zn (45.0 Ω). These findings confirm the superior charge transfer ability of the Ni-0.1W@Zn anode. The reduced impedance highlights enhanced Zn^{2+} ion transference number and improved charge transfer kinetics, both critical for achieving stable and uniform Zn plating/stripping. The incorporation of tungsten generates a uniform electric field across the electrode surface, enabling homogeneous Zn deposition while effectively suppressing dendrite formation. This well-regulated deposition mechanism ensures efficient Zn cycling and high reversibility, contributing to the improved cycling stability of the Ni-0.1W@Zn anode. These results underscore the importance of the Ni-W coating in optimizing Zn^{2+} transport, stabilizing Zn deposition, and addressing challenges in Zn-ion battery performance and durability.

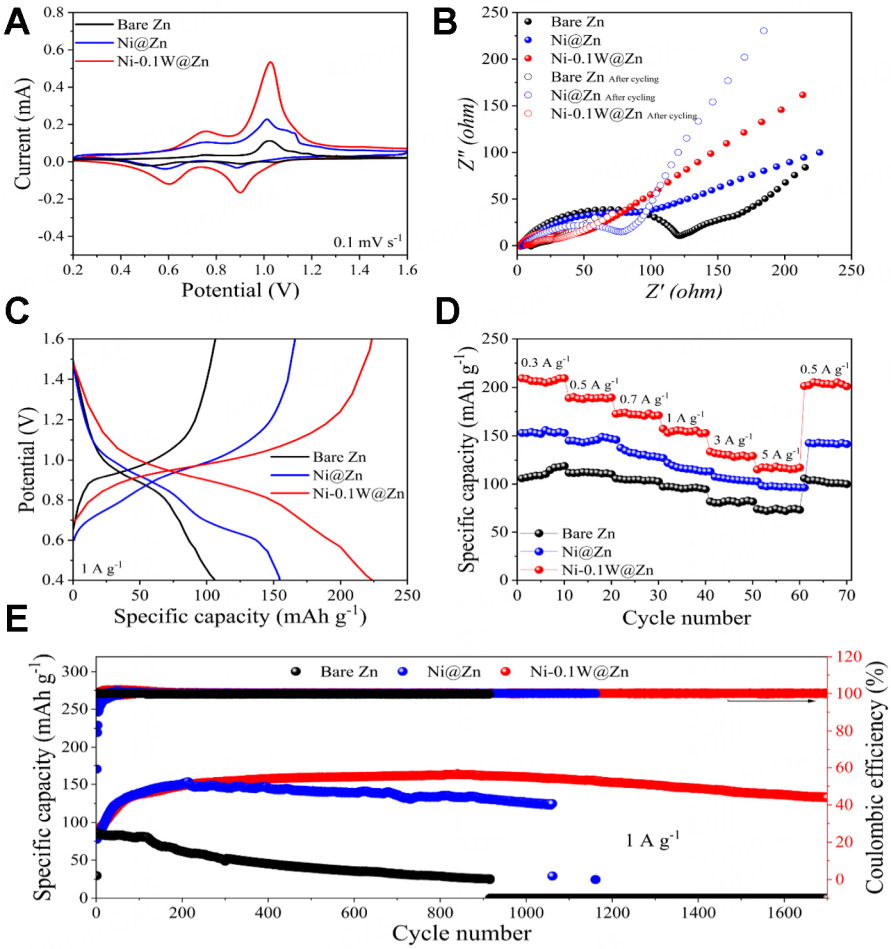

Figure 5. (A) CV curves of Bare-Zn// V_2O_5, Ni@Zn//V_2O_5 and Ni-0.1W@Zn//V_2O_5; (B) EIS curves of Bare-Zn//V_2O_5, Ni@Zn//V_2O_5 and Ni-0.1W@Zn//V_2O_5; (C) Charge and discharge curves of Bare-Zn//V_2O_5, Ni@Zn//V_2O_5 and Ni-0.1W@Zn//V_2O_5; (D) Rate performances of Bare-Zn//V_2O_5, Ni@Zn//V_2O_5 and Ni-0.1W@Zn//V_2O_5; and (E) Cycling stabilities of Bare-Zn//V_2O_5, Ni@Zn//V_2O_5 and Ni-0.1W@Zn//V_2O_5 at 1 mA cm^{-2}.

The charge/discharge profiles of full cells at a current density of 0.3 A g^{-1}, as shown in Figure 5C, reveal significant differences in specific capacity among the electrodes. The bare Zn anode achieves a discharge specific capacity of 117.33 mAh g^{-1}, while the Ni@Zn anode reaches 150.06 mAh g^{-1}.

Notably, the Ni-0.1W@Zn anode delivers the highest discharge specific capacity of 210.42 mAh g^{-1}, demonstrating its ability to significantly enhance reversible capacity through improved Zn plating/stripping behavior. Furthermore, the Ni-0.1W@Zn anode exhibits substantially reduced voltage polarization compared to both bare Zn and Ni@Zn electrodes, aligning with CV results and further validating its superior electrochemical performance. High-rate performance testing Figure 5D shows that the Ni-0.1W@Zn battery achieves an initial capacity of 210.42 mAh g^{-1} at 0.3 A g^{-1} and maintains capacity even at 5.0 A g^{-1} [Supplementary Figure 13]. The Ni-0.1W@Zn||V_2O_5 batteries exhibit significantly improved long-term cycling performance compared to bare Zn||V_2O_5 and Ni@Zn||V_2O_5 batteries. At 1 A g^{-1}, the Ni-0.1W@Zn anode achieves a specific capacity of 163 mAh g^{-1} with capacity retention exceeding 81% after 1,500 cycles [Figure 5E]. At a lower current density of 0.5 A g^{-1} [Supplementary Figure 14], the Ni-0.1W@Zn anode demonstrates excellent stability, retaining 89% of its capacity after 1,000 cycles. These results highlight the consistent electrochemical performance of the Ni-0.1W@Zn anode across varied operating

conditions. Combined with its outstanding performance at 1 A g^{-1}, the Ni-0.1W@Zn system demonstrates versatility and durability, making it a promising candidate for advanced Zn-ion battery applications. In contrast, bare Zn||V_2O_5 and Ni@Zn||V_2O_5 batteries show rapid capacity loss and structural degradation caused by dendrite growth and ongoing corrosion during extended cycling. Morphological analysis reveals that the Ni-0.1W@Zn anode maintains a smooth and uniform surface even after prolonged cycling [Supplementary Figure 15], while bare Zn anodes develop rough, vertically grown Zn flakes, exacerbating dendrite formation. These findings emphasize the role of the Ni-W coating in suppressing dendrite growth and minimizing side reactions, key factors in enhancing cycling stability and extending the lifespan of Zn-ion batteries. Collectively, these results confirm that the Ni-0.1W@Zn anode is a durable and efficient solution for advancing Zn-ion battery technology, offering a pathway toward reliable, long-lasting energy storage systems.

CONCLUSIONS

In summary, we successfully developed a nanocrystalline Ni-W layer on Zn foil that directs Zn deposition along specific crystal planes, effectively minimizing corrosion and suppressing by-product formation. This modification significantly enhances Zn^{2+}/Zn reversibility, presenting strong potential for stable and high-performance AZIBs. Optimal performance was achieved using a 0.1 M Ni-W concentration with a 300 s deposition time, producing favorable surface properties and improved battery performance. The Ni-0.1W@Zn anode demonstrated exceptional cycling stability, enabling symmetric cells to operate for over 2,000 h at a current density of 1 mA cm^{-2} with a high CE of 98%. Additionally, these electrodes consistently outperformed both Ni@Zn and bare Zn anodes, underscoring their practicality for energy storage applications.

The nanocrystalline Ni-W coating plays a pivotal role in advancing Zn-ion battery performance by providing a uniform and compact surface that facilitates controlled Zn deposition, suppresses dendrite formation, and reduces by-product accumulation. Its superior corrosion resistance protects the Zn substrate during prolonged cycling, while its excellent electrical conductivity ensures efficient electron transport. These synergistic features enhance structural stability and enable consistent Zn plating and stripping, resulting in a longer battery lifespan and improved operational safety.

This study presents a transformative approach to overcoming the challenges associated with zinc anodes through the integration of a scalable and practical Ni-W coating. The exceptional electrochemical stability, enhanced durability, and dendrite suppression demonstrated by the Ni-0.1W@Zn anode highlight its critical importance in the development of sustainable and high-efficiency energy storage solutions. By bridging the gap between laboratory research and industrial application, this work establishes a promising foundation for next-generation battery technologies essential to the future of renewable energy systems.

DECLARATIONS

Author's contributions

Sample fabrication and characterization: Choonha-Anothai, K.; Yang, C.

Data analysis and interpretation: Choonha-Anothai, K.; Yang, C.; Wang, M.; Dai, Z.; Kiatwisarnkij, N.; Lolupiman, K.; Qin, J.

Preparation of the manuscript and discussion: Choonha-Anothai, K.; Yang, C.; Wang, M.; Dai, Z.; Zhang, X.; Wangyao, P.; Qin, J.

Availability of data and materials

The data supporting the findings of this study are available within this Article and its Supplementary Materials. Further data are available from the corresponding authors upon request.

Financial support and sponsorship

This work was supported by the Thailand Science Research and Innovation Fund Chulalongkorn University (INDFF682266200010), National Research Council of Thailand (NRCT) and Chulalongkorn University (N42A660383), and National Natural Science Foundation of China (Grant Nos. 52125405 and U22A20108).

Conflicts of interest

All authors declared that there are no conflicts of interest.

Ethical approval and consent to participate

Not applicable.

Consent for publication

Not applicable.

REFERENCES

1. Arévalo-Cid, P.; Dias, P.; Mendes, A.; Azevedo, J. Redox flow batteries: a new frontier on energy storage. *Sustain. Energy. Fuels.* **2021**, *5*, 5366-419. DOI
2. Shin, J.; Lee, J.; Park, Y.; Choi, J. W. Aqueous zinc ion batteries: focus on zinc metal anodes. *Chem. Sci.* **2020**, *11*, 2028-44. DOI PubMed PMC
3. Ghosh, M.; Vijayakumar, V.; Kurungot, S. Dendrite growth suppression by Zn^{2+}-integrated nafion ionomer membranes: beyond porous separators toward aqueous Zn/V_2O_5 batteries with extended cycle life. *Energy. Technol.* **2019**, *7*, 1900442. DOI
4. Chen, S.; Ying, Y.; Ma, L.; et al. An asymmetric electrolyte to simultaneously meet contradictory requirements of anode and cathode. *Nat. Commun.* **2023**, *14*, 2925. DOI PubMed PMC
5. Olbasa, B. W.; Fenta, F. W.; Chiu, S. F.; et al. High-rate and long-cycle stability with a dendrite-free zinc anode in an aqueous Zn-ion battery using concentrated electrolytes. *ACS. Appl. Energy. Mater.* **2020**, *3*, 4499-508. DOI
6. Liu, X.; Guo, Y.; Ning, F.; et al. Fundamental understanding of hydrogen evolution reaction on zinc anode surface: a first-principles study. *Nanomicro. Lett.* **2024**, *16*, 111. DOI PubMed PMC
7. Cai, Z.; Wang, J.; Sun, Y. Anode corrosion in aqueous Zn metal batteries. *eScience* **2023**, *3*, 100093. DOI
8. Qin, H.; Kuang, W.; Hu, N.; et al. Building metal-molecule interface towards stable and reversible Zn metal anodes for aqueous rechargeable zinc batteries. *Adv. Funct. Mater.* **2022**, *32*, 2206695. DOI
9. Rosen, M. A.; Farsi, A. Battery technology: from fundamentals to thermal behavior and management. 2023. Available from: https://books.google.co.th/books?id=YpGoEAAAQBAJ [Last accessed on 18 Apr 2025]
10. Liu, Z.; Zhou, W.; He, J.; et al. Binder-free MnO_2 as a high rate capability cathode for aqueous magnesium ion battery. *J. Alloys. Compd.* **2021**, *869*, 159279. DOI
11. Zhang, N.; Wang, J.; Liu, X.; et al. Towards high-performance aqueous Zn-MnO_2 batteries: formation mechanism and alleviation strategies of irreversible inert phases. *Compos. Part. B. Eng.* **2023**, *260*, 110770. DOI
12. Hu, P.; Yan, M.; Zhu, T.; et al. Zn/V_2O_5 aqueous hybrid-ion battery with high voltage platform and long cycle life. *ACS. Appl. Mater. Interfaces.* **2017**, *9*, 42717-22. DOI
13. He, H. B.; Liu, Z.; Luo, Z. X.; Zhang, Z. H.; Chen, Y.; Zeng, J. Sustainable porous biochar coated MnO_2 composites as the cathode in aqueous Zn/Mn batteries. *J. Alloys. Compd.* **2023**, *960*, 170853. DOI
14. Feng, K.; Wang, D.; Yu, Y. Progress and prospect of Zn anode modification in aqueous zinc-ion batteries: experimental and theoretical aspects. *Molecules* **2023**, *28*, 2721. DOI PubMed PMC
15. Chen, Y.; Li, J.; Zhang, S.; Cui, J.; Shao, M. Highly reversible zinc anode enhanced by ultrathin MnO_2 cathode material film for high-performance zinc-ion batteries. *Adv. Mater. Inter.* **2020**, *7*, 2000510. DOI
16. Cao, J.; Wang, X.; Qian, S.; et al. De-passivation and surface crystal plane reconstruction via chemical polishing for highly reversible zinc anodes. *Adv. Mater.* **2024**, *36*, e2410947. DOI
17. Shang, Z.; Qi, H.; Liu, X.; Ouyang, C.; Wang, Y. Structural optimization of lithium-ion battery for improving thermal performance

based on a liquid cooling system. *Int. J. Heat. Mass. Transfer.* **2019**, *130*, 33-41. DOI

18. Yang, S.; Du, H.; Li, Y.; et al. Advances in the structure design of substrate materials for zinc anode of aqueous zinc ion batteries. *Green. Energy. Environ.* **2023**, *8*, 1531-52. DOI
19. Wang, M.; Dai, Z.; Yang, C.; et al. Boosting de-solvation via halloysite nanotubes-cellulose composite separator for dendrite-free zinc anodes. *Mater. Today. Energy.* **2024**, *46*, 101736. DOI
20. Yin, C.; Pan, C.; Pan, Y.; Hu, J. Hierarchical spheroidal MOF-derived MnO@C as cathode components for high-performance aqueous zinc ion batteries. *J. Colloid. Interface. Sci.* **2023**, *642*, 513-22. DOI
21. Carvalho, M. L.; Mela, G.; Temporelli, A.; Brivio, E.; Girardi, P. Sodium-ion batteries with $Ti_1Al_1TiC_{1.85}$ MXene as negative electrode: life cycle assessment and life critical resource use analysis. *Sustainability* **2022**, *14*, 5976. DOI
22. Zhang, Y.; Bi, S.; Niu, Z.; Zhou, W.; Xie, S. Design of Zn anode protection materials for mild aqueous Zn-ion batteries. *Energy. Mater.* **2022**, *2*, 200012. DOI
23. Li, Y.; Guo, Y.; Li, Z.; Wang, P.; Xie, Y.; Yi, T. Carbon-based nanomaterials for stabilizing zinc metal anodes towards high-performance aqueous zinc-ion batteries. *Energy. Storage. Mater.* **2024**, *67*, 103300. DOI
24. Liu, M.; Tian, C.; Zhang, D.; et al. Design on modified-zinc anode with dendrite- and side reactions-free by hydrophobic organic-inorganic hybrids for ultra-stable zinc ion batteries. *Nano. Energy.* **2022**, *103*, 107805. DOI
25. Zhou, X.; Chen, R.; Cui, E.; et al. A novel hydrophobic-zincophilic bifunctional layer for stable Zn metal anodes. *Energy. Storage. Mater.* **2023**, *55*, 538-45. DOI
26. Xu, W.; Wang, Y. Recent progress on zinc-ion rechargeable batteries. *Nanomicro. Lett.* **2019**, *11*, 90. DOI PubMed PMC
27. Naveed, A.; Ali, A.; Rasheed, T.; et al. Revisiting recent and traditional strategies for surface protection of Zn metal anode. *J. Power. Sources.* **2022**, *525*, 231122. DOI
28. Mo, F.; He, N.; Chen, L.; et al. Strategies for stabilization of Zn anodes for aqueous Zn-based batteries: a mini review. *Front. Chem.* **2021**, *9*, 822624. DOI PubMed PMC
29. Kothanam, N.; Harachai, K.; Hom-On, C.; et al. Enhanced particle incorporation for co-electrodeposited Ni-P/diamond coatings with a pulse-stirring technique. *App. Surf. Sci. Adv.* **2023**, *18*, 100499. DOI
30. Wilcox, G.; Gabe, D. Electrodeposited zinc alloy coatings. *Corros. Sci.* **1993**, *35*, 1251-8. DOI
31. Nady, H.; Negem, M. Electroplated Zn-Ni nanocrystalline alloys as an efficient electrocatalyst cathode for the generation of hydrogen fuel in acid medium. *Int. J. Hydrogen. Energy.* **2018**, *43*, 4942-50. DOI
32. Lotfi, N.; Aliofkhazraei, M.; Rahmani, H.; Darband, G. B. Zinc-nickel alloy electrodeposition: characterization, properties, multilayers and composites. *Prot. Met. Phys. Chem. Surf.* **2018**, *54*, 1102-40. DOI
33. Bernasconi, R.; Panzeri, G.; Firtin, G.; Kahyaoglu, B.; Nobili, L.; Magagnin, L. Electrodeposition of ZnNi alloys from choline chloride/ethylene glycol deep eutectic solvent and pure ethylene glycol for corrosion protection. *J. Phys. Chem. B.* **2020**, *124*, 10739-51. DOI PubMed PMC
34. Hristova, E.; Mitov, M.; Rashkov, R.; Arnaudova, M.; Popov, A. Sulphide oxidation on electrodeposited Ni-Mo-W catalysts. *Bulg. Chem. Commun.* **2008**, *40*, 291-4. Available from: http://www.bcc.bas.bg/bcc_volumes/volume_40_number_3_2008/Volume_40_Number_3_2008_PDF/2826-AC.pdf [Last accessed on 16 Apr 2025]
35. Allahyarzadeh, M.; Aliofkhazraei, M.; Rezvanian, A.; Torabinejad, V.; Sabour, R. A. Ni-W electrodeposited coatings: characterization, properties and applications. *Surf. Coat. Technol.* **2016**, *307*, 978-1010. DOI
36. Tasić, G. S.; Lačnjevac, U.; Tasić, M. M.; et al. Influence of electrodeposition parameters of Ni-W on Ni cathode for alkaline water electrolyser. *Int. J. Hydrogen. Energy.* **2013**, *38*, 4291-7. DOI
37. Zhang, X.; Qin, J.; Perasinjaroen, T.; et al. Preparation and hardness of pulse electrodeposited Ni-W-diamond composite coatings. *Surf. Coat. Technol.* **2015**, *276*, 228-32. DOI
38. Kazimierczak, H.; Eliaz, N. Induced codeposition of tungsten with zinc from aqueous citrate electrolytes. *Coatings* **2023**, *13*, 2001. DOI
39. Cao, J.; Zhang, D.; Yue, Y.; et al. Strongly coupled tungsten oxide/carbide heterogeneous hybrid for ultrastable aqueous rocking-chair zinc-ion batteries. *Chem. Eng. J.* **2021**, *426*, 131893. DOI
40. Pletcher, D.; Walsh, F. C. Industrial electrochemistry, 2nd ed. Chapman and Hall; 1990. Available from: https://books.google.co.th/books?id=E_u9ARrm37oC [Last accessed on 18 Apr 2025]
41. Sunwang, N.; Wangyao, P.; Boonyongmaneerat, Y. The effects of heat treatments on hardness and wear resistance in Ni-W alloy coatings. *Surf. Coat. Technol.* **2011**, *206*, 1096-101. DOI
42. Elias, L.; Chitharanjan, H. A. Electrodeposition of laminar coatings of Ni-W alloy and their corrosion behaviour. *Surf. Coat. Technol.* **2015**, *283*, 61-9. DOI
43. Li, B.; Li, G.; Zhang, D.; et al. Unveiling the impact of the polypyrrole coating layer thickness on the electrochemical performances of $LiNi_{0.5}Co_{0.2}Mn_{0.3}O_2$ in Li-ion battery. *ChemistrySelect* **2019**, *4*, 6354-60. DOI
44. He, H.; Qin, H.; Wu, J.; et al. Engineering interfacial layers to enable Zn metal anodes for aqueous zinc-ion batteries. *Energy. Storage. Mater.* **2021**, *43*, 317-36. DOI
45. You, Y.; Fang, G.; Fan, M.; Guo, J.; Li, Q.; Wan, J. Leveraging novel microwave techniques for tailoring the microstructure of energy storage materials. *Microstructures* **2024**, *4*, 2024035. DOI
46. Baek, M.; Kim, J.; Jeong, K.; et al. Naked metallic skin for homo-epitaxial deposition in lithium metal batteries. *Nat. Commun.* **2023**, *14*, 1296. DOI PubMed PMC

47. Guo, X.; Zhang, Z.; Li, J.; et al. Alleviation of dendrite formation on zinc anodes via electrolyte additives. *ACS. Energy. Lett.* **2021**, *6*, 395-403. DOI
48. Ma, L.; Zhi, C. Zn electrode/electrolyte interfaces of Zn batteries: a mini review. *Electrochem. Commun.* **2021**, *122*, 106898. DOI
49. Li, T.; Yan, S.; Dong, H.; et al. Engineering hydrophobic protective layers on zinc anodes for enhanced performance in aqueous zinc-ion batteries. *J. Energy. Chem.* **2024**, *97*, 1-11. DOI
50. Deng, S.; Xu, B.; Zhao, J.; Fu, H. Advanced design for anti-freezing aqueous zinc-ion batteries. *Energy. Storage. Mater.* **2024**, *70*, 103490. DOI
51. Xu, W.; Zhang, M.; Dong, Y.; Zhao, J. Two-dimensional materials for dendrite-free zinc metal anodes in aqueous zinc batteries. *Batteries* **2022**, *8*, 293. DOI
52. Cao, J.; Wu, H.; Zhang, D.; et al. In-situ ultrafast construction of zinc tungstate interface layer for highly reversible zinc anodes. *Angew. Chem. Int. Ed.* **2024**, *63*, e202319661. DOI
53. Zuo, Y.; Wang, K.; Pei, P.; et al. Zinc dendrite growth and inhibition strategies. *Mater. Today. Energy.* **2021**, *20*, 100692. DOI
54. Song, Z.; Yang, C.; Kiatwisarnkij, N.; et al. Polyethylene glycol-protected zinc microwall arrays for stable zinc anodes. *ACS. Appl. Mater. Interfaces.* **2024**, *16*, 64834-45. DOI PubMed PMC
55. Zhang, H.; Li, F.; Li, Z.; Gao, L.; Xu, B.; Wang, C. Surface modification induces oriented Zn(002) deposition for highly stable zinc anode. *Batteries* **2024**, *10*, 178. DOI
56. Yang, C.; Woottapanit, P.; Geng, S.; et al. Highly reversible Zn anode design through oriented ZnO(002) facets. *Adv. Mater.* **2024**, *36*, e2408908. DOI PubMed PMC
57. Lim, W. G.; Li, X.; Reed, D. Understanding the role of zinc hydroxide sulfate and its analogues in mildly acidic aqueous zinc batteries: a review. *Small. Methods.* **2024**, *8*, e2300965. DOI PubMed
58. Shang, Y.; Kundu, D. Understanding and performance of the zinc anode cycling in aqueous zinc-ion batteries and a roadmap for the future. *Batteries. Supercaps.* **2022**, *5*, e202100394. DOI
59. Luo, M.; Wang, C.; Lu, H.; et al. Dendrite-free zinc anode enabled by zinc-chelating chemistry. *Energy. Storage. Mater.* **2021**, *41*, 515-21. DOI